communications biology

Article

https://doi.org/10.1038/s42003-024-07179-1

Modulation of ATM enhances DNA repair in G2/M phase of cell cycle and averts senescence in Fuchs endothelial corneal dystrophy

Check for updates

Shazia Ashraf[1,2], Neha Deshpande[1,2], Queenie Cheung[1], Jeffrey Boakye Asabere[1], Raymond Jeff Wong[1], Alex G. Gauthier[1], Mohit Parekh[1], Yadav Adhikari[1], Geetha Melangath[1] & Ula V. Jurkunas[1]

Fuchs Endothelial Corneal Dystrophy (FECD) is an aging disorder characterized by expedited loss of corneal endothelial cells (CEnCs) and heightened DNA damage compared to normal CEnCs. We previously established that ultraviolet-A (UVA) light causes DNA damage and leads to FECD phenotype in a non-genetic mouse model. Here, we demonstrate that acute treatment with chemical stressor, menadione, or physiological stressors, UVA, and catechol estrogen (4-OHE_2), results in an early and increased activation of ATM-mediated DNA damage response in FECD compared to normal CEnCs. Acute stress with UVA and 4OHE_2 causes (i) greater cell-cycle arrest and DNA repair in G2/M phase, and (ii) greater cytoprotective senescence in *NQO1*$^{-/-}$ compared to *NQO1*$^{+/+}$ cells, which was reversed upon ATM inhibition. Chronic stress with UVA and 4OHE_2 results in ATM-driven cell-cycle arrest in G0/G1 phase, reduced DNA repair, and cytotoxic senescence, due to sustained damage. Likewise, UVA-induced cell-cycle reentry, gamma-H2AX foci, and senescence-associated heterochromatin were reduced in Atm-null mice. Remarkably, inhibiting ATM activation with KU-55933 restored DNA repair in G2/M phase and attenuated senescence in chronic cellular model of FECD lacking NQO1. This study provides insights into understanding the pivotal role of ATM in regulating cell-cycle, DNA repair, and senescence, in oxidative-stress disorders like FECD.

Corneal endothelial cells (CEnCs) form a hexagonal monolayer in the posterior cornea and serve a central role in maintaining corneal clarity and hydration by constant pumping of ions between the stroma and aqueous fluid[1,2]. Derived from the neural crest, CEnCs are arrested in the post-mitotic state[3,4] and show minimal proliferation in vivo with 4000 cells/mm^2 at birth that gradually decreases with age. Fuchs endothelial corneal dystrophy (FECD), the most common cause of corneal endothelial degeneration, is an age-related genetically heterogeneous disease resulting in the accelerated loss of CEnCs leading to corneal edema and loss of vision[5]. FECD affects 4% of the U.S. population over the age of 40 years and is the leading indication for the corneal transplantations performed in the U.S., which is currently the only treatment option available for this disease[6–8]. It is characterized by mitochondrial dysfunction, profibrotic extracellular matrix deposits forming dome shaped excrescences called guttae protruding from the Descemet's membrane, and ensuing CEnC apoptosis[9–11]. Notable, FECD exhibits a pronounced predominance for females[12–14], suggesting a potential hormonal involvement in the disease pathogenesis.

Due to high metabolic activity, inability to replicate the genome, and lifelong exposure to ultraviolet light, the mitochondria-rich CEnCs are highly susceptible to ROS-mediated DNA damage[15]. Very little is known about the protective mechanisms by which normal CEnCs detect and repair DNA damage, thereby facilitating their longevity. The DDR signal transduction pathway is orchestrated by upstream central kinases such as ATM (ataxia-telangiectasia mutated), ATR (ATM and Rad3-Related) and DNA-PKcs (DNA–dependent protein kinase) which, upon activation by DNA damage, phosphorylates and activates downstream effectors that are involved in DNA repair, cell-cycle arrest, senescence, or apoptosis[16]. ATM has been shown to play a central role in controlling the DNA damage response leading to cell cycle activation of postmitotic cells, like neurons[17–19]. Several studies have shown that ATM but not ATR is essential for the

[1]Schepens Eye Research Institute of Massachusetts Eye and Ear, Department of Ophthalmology, Harvard Medical School, Boston, MA, 02114, USA. [2]These authors contributed equally: Shazia Ashraf, Neha Deshpande. e-mail: ula_jurkunas@meei.harvard.edu

upregulation of p21 and the G1 cell cycle checkpoint[20] and activation of senescence[21,22]. ATM responds to DNA double-stranded breaks (DSBs), which may be caused intrinsically through the collapse of stalled replication fork or extrinsically through exposure to ionizing radiation (IR)[23]. Despite great advancements in our understanding of ATM signaling and function in recent years, the complex mechanisms involved in its activation and response are not fully resolved.

ATM is a 370 kDa serine/threonine kinase belonging to the phosphatidyl inositol 3-kinase (PI3K) family[24,25]. In its inactive form, ATM forms homodimers which dissociate into catalytically active monomers following rapid intermolecular autophosphorylation of serine1981 (pATM-S1981) upon ATM activation[26]. Since the initial discovery of its autophosphorylation site and its role in ATM activation, other ATM post-translational modifications have been reported[27,28]. The MRN (MRE11-RAD50-NBS1) complex recruits ATM to the site of DSBs[29], where it acts as a damage sensor that can also form a physical bridge spanning the DSBs[30]. Activated ATM phosphorylates histone variant H2AX at serine139 (γH2AX-S139) within minutes after DNA damage, forming γH2AX foci which enables the recruitment of numerous DNA repair proteins and chromatin remodeling complexes around DSBs[31,32]. ATM is generally regarded as the principal mediator of the G1/S cell cycle checkpoint, which prevents cells with damaged DNA from entering S-phase. In response to induction of DNA-DSBs, ATM directly phosphorylates tumor suppressor protein p53 on serine15 (pp53-S15)[33] thereby stabilizing p53. Additionally, pATM-S1981 activates cell cycle checkpoint protein Chk2 at threonine68 (pChk2-T68) that in turn phosphorylates p53 at serine20 (pp53-S20)[34]. This phosphorylation at p53 leads to its stabilization by preventing its Mdm2-mediated ubiquitination and degradation[34,35]. Activated p53 acts as a transcription factor and drives the expression of genes involved in cell cycle checkpoint activation, such as p21, but also several genes which are involved in the induction of apoptosis. resulting in cell cycle arrest[36,37]. In addition to its role in the G1/S checkpoint, ATM also contributes to the activation of the intra-S phase and G2/M cell cycle arrest, as cells deficient in ATM do not reduce DNA synthesis following induction of DNA-DSBs, referred as radioresistant DNA synthesis[38,39].

Previous studies have demonstrated that in response to oxidative stress, various substrates are phosphorylated in an ATM-dependent manner, thus demonstrating the complexity of the ATM-mediated DDR pathways[40,41]. Deficiency of ATM in humans results in the neurodegenerative disorder, Ataxia-telangiectasia, characterized by loss of Purkinje neurons, immunodeficiencies, hypersensitivity to ionizing radiations and predisposition to cancer[42]. Furthermore, reactive oxygen species (ROS) has been shown to directly trigger ATM autophosphorylation and facilitate its localization to DSBs[43]. While mechanisms of DDR are well studied in proliferating cells, DDR signaling pathways in post-mitotically arrested cells, specifically CEnCs that are particularly prone to oxidative stress-mediated damage, remain unclear. In this study, we investigate the role of oxidative stress induced by a chemical stressor menadione, as well as a physiological stressor UVA irradiation, in ATM-mediated DDR signaling in normal and diseased CEnCs. Since FECD is more pronounced in females[14], we also investigate a combined effect of UVA and catechol estrogen (4-OHE_2), a by-product of estrogen metabolism, in elucidating the role of ATM in the progression of FECD. Our previous studies demonstrated that NQO1 is downregulated in FECD specimens as well as FECD cell lines[44] compared to controls. Downregulation of NQO1 exacerbated menadione induced oxidative stress leading to endothelial-mesenchymal transition in corneal endothelial cells[10]. Additionally, we showed that NQO1-null mice exhibited greater CE cell loss, greater ROS production, and lack of neutralization of reactive estrogen metabolites due to loss of NQO1[14], mimicking end-stage FECD. Herein, we therefore utilized our previously generated NQO1-null (*NQO1*$^{-/-}$) stable cell lines[10] as a cellular model of FECD in addition to patient derived cell lines, to study ATM-mediated DDR signaling under acute and chronic oxidative stress. We demonstrate using our in-vitro and in vivo FECD models that effectors of DDR signaling determine the extent of cell cycle arrest, DNA repair, or senescence based on the duration of the stress and DNA damage. By using ATM inhibitor – KU-55933, we show that modulation of DDR signaling may have a potential therapeutic application in averting senescence in diseased CEnCs.

Results

Menadione-induced oxidative stress causes earlier and greater activation of ATM-mediated DDR leading to elevated S-phase in FECD cells

Previously, we established that chemical stressor, menadione (MN) induces intracellular ROS in CEnCs and causes pathophysiological changes seen in FECD[9]. To determine the time-kinetics of ROS-induced DDR activation in CEnCs, we treated SVN1-67F (normal) and SVF1-73F (FECD) cells, with 25 μM MN and assessed the levels of DDR proteins by western blotting at 30, 60, 90 and 120 min of treatment. MN induced a time-dependent activation of ATM *via* autophosphorylation at S1981 (pATM), DNA damage marker H2AX *via* phosphorylation at S139 (pH2AX), and cell-cycle checkpoint regulators p53 and Chk2 *via* phosphorylation at S15 (pp53) and T68 (pChk2) respectively (Fig. 1a). In SVF1-73F cells, levels of pATM/ATM, pH2AX/H2AX, pp53/p53, and pChk2/Chk2 exhibited peak activation as early as at 60 min and declined at 90 and 120 min, while in SVN1-67F cells, pATM/ATM levels peaked only later at 120 min without significant activation of pH2AX/H2AX and pp53/p53 yet, thereby establishing 60 min as the timepoint of greatest differential ATM-mediated DDR activation between the two cell lines (Fig. 1a, Supplementary Fig. 1). At 60 min, MN caused cell elongation and formation of rosette-like structures and long processes, characteristic of FECD morphology[9,45], distinctly in SVF1-73F cells (Supplementary Fig. 2a) and induced a marked increase in the levels of pATM/ATM (4-fold), pH2AX/H2AX (4-fold), and pp53/p53 (3.6-fold), predominantly in SVF1-73F cells, whereas MN upregulated pChk2/Chk2 levels in both SVF1-73F (1.6-fold) and SVN1-67F (2.8-fold) cells at this timepoint (Fig. 1b). We found lack of activation of another key DDR kinase, ATR, after MN treatment as indicated by the unchanged pATR/ATR levels across all timepoints in both SVN1-67F and SVF1-73F cells (Supplementary Fig. 2b). Furthermore, immunoprecipitation assay using pATM antibody, but not IgG antibody (negative control) at 60 min of MN treatment resulted in an increased pull down of pATM along with an enhanced co-immunoprecipitation of pp53-S15, a direct substrate of pATM, in SVF1-73F compared to SVN1-67F cells (Fig. 1c, Supplementary Fig. 3a). Additionally, immunoprecipitation with total ATM antibody demonstrated an increased pull down of total p53 in SVF1-73F compared to SVN1-67F cells (Supplementary Fig. 4). We further employed a specific and potent ATM kinase inhibitor, KU-55933[46], to examine whether MN-induced activation of p53 is dependent on the ATM protein kinase. KU-55933, at 20 μM concentration, determined from a dose response curve (Supplementary Fig. 5a), completely ablated the MN-induced phosphorylation of ATM (S1981) and p53 (S15) (Fig. 1d, Supplementary Fig. 3b) as well as H2AX (S139) and Chk2 (T68) (Supplementary Fig. 5b) in both SVN1-67F and SVF1-73F indicating that ATM plays a major role in transducing the MN-induced DNA damage signaling in CEnCs. We confirmed our finding of increased pATM/ATM activation in FECD compared to normal cells using an additional normal cell line, SVN2-67F, as well as an additional FECD cell line, SVF5-54F treated with MN (Supplementary Fig. 5c). ATM is known to be involved in mediating the halting of cell cycle progression in response to oxidative stress-mediated DNA damage[47], however, little is known about its role in cell cycle regulation in the context of FECD pathogenesis. We therefore assayed the cell cycle profiles post MN treatment of normal SVN1-67F, and FECD SVF1-73F and SVF5-54F cells. Treatment with 50 μM MN for 1 hour followed by a 24 h recovery period caused a marked increase in the S-phase population of FECD cells SVF1-73F (3-fold) and SVF5-54F (6-fold), compared to normal cells SVN1-67F (2-fold) (Fig. 1e, f; Supplementary Fig. 6). There was no difference in the cell doubling times of the normal cell line, SVN1-67F, and the two FECD cell lines, SVF1-73F and SVF5-54F, confirming that the differential S-phase accumulation was not an effect of different proliferations rates between the cell lines (Supplementary Fig. 7).Taken together, these results demonstrate the involvement of the ATM-p53-H2AX axis which is activated earlier and to a greater extent in

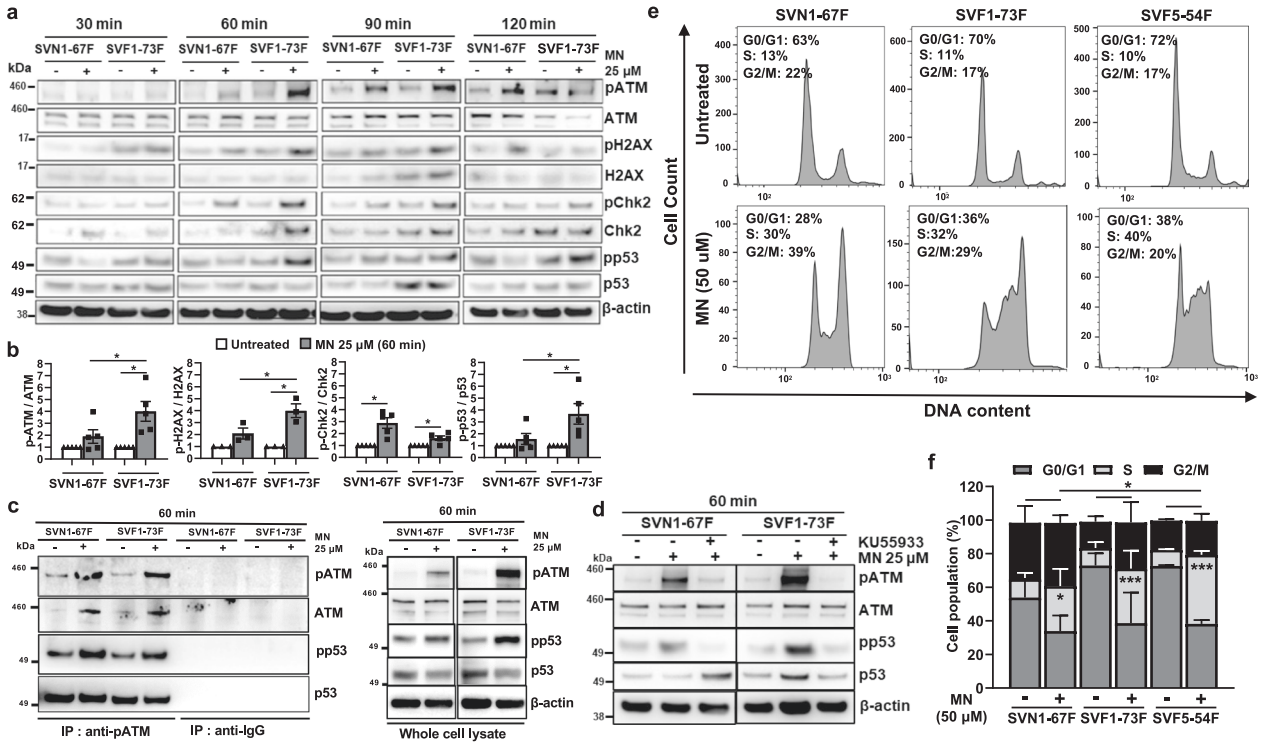

Fig. 1 | FECD cells show greater activation of ATM-mediated DDR than normal CEnCs in response to menadione-induced chemical stress. a Western blot of time course of MN (25 μM)-induced DDR activation shows earlier and greater activation of phospho-ATM (pATM/ATM) and its downstream effector proteins (pH2AX/H2AX, pp53/p53, and pChk2/Chk2) in SVF1-73F compared to SVN1-67F cells. **b** Fold change in densitometry of MN- over un-treated cells shows significantly greater activation of pATM/ATM, pp53/p53, and pH2AX/H2AX, but not pChk2/Chk2 proteins in SVF1-73F compared to SVN1-67F at 60 min of treatment with 25 μM MN. *$P < 0.05$ applying paired *t*-test. **c** Immunoprecipitation with anti-pATMS1981 or IgG antibody and immunoblotting from whole cell lysates prepared after treatment with 25 μM MN for 60 min shows greater pulldown of pATM/ATM and pp53/p53 in SVF1-73F compared to SVN1-67F cells. Western blotting of whole cell lysates shows greater pATM/ATM and pp53/p53 expression levels in SVF1-73F compared to SVN1-67F cells after MN treatment. **d** Western blotting at 60 min after co-treatment with MN (25 μM) and ATM inhibitor, KU-55933 (20 μM) shows depleted levels of pATM/ATM and pp53/p53 affirming ATM-driven DDR activation. **e** Cell cycle phase histograms of normal cells, SVN1-67F, and FECD cells, SVF1-73F and SVF5-54F, stained with propidium iodide and subjected to flow cytometry demonstrate an increase in the S-phase distribution of all three cell lines 24 h after treatment with 50 μM MN compared to no treatment. **f** Inter-cell line comparison of percentage cells in each phase of the cell cycle shows a significantly elevated S-phase in SVF5-54F compared to SVN1-67F cells 24 h after MN treatment. ***, * indicates $P < 0.001$, or < 0.05 respectively applying one-way ANOVA with Tukey's Multiple Comparison Test comparing the S-phase of each group. Data represented as mean ± SEM of N ≥ 3.

FECD leading to an elevated S-phase in response to MN-induced oxidative stress.

UVA light induced oxidative stress causes ATM-mediated G2/M-phase arrest in FECD cells

We sought to determine whether the environmental stressor UVA light also causes an early ATM activation in FECD cells compared to normal CEnCs. The effect of female sex was assessed by treatment of cells with catechol estrogen found to be increased in FECD[14]. Both SVN1-67F (normal) and SVF1-73F (FECD) cells were exposed to UVA (10 J/cm^2 or 25 J/cm^2) with and without 4-OHE$_2$ (10 μM). Western blot analysis with 10 J/cm^2, but not 25 J/cm^2, showed that UVA + 4-OHE$_2$ caused greater activation of pATM/ATM (2-fold, $p < 0.01$) and pChk2/Chk2 (2.5-fold, $p < 0.001$) in SVF1-73F, but not in SVN1-67F compared to no treatment (Fig. 2a, b; Supplementary Fig. 8, Supplementary Fig. 9). To investigate the cell cycle status of treated cells compared to untreated, cells in each phase of the cell cycle were quantified using flow cytometry based on fluorescence intensity of propidium iodide labelled DNA content (Fig. 2c). Exposure to UVA + 4-OHE$_2$ compared to no treatment induced a marked increase in G2/M phase arrest in SVN1-67F (2-fold; 44% *vs* 22%) and in SVF1-73F (2.7-fold; 51% *vs* 19%) at 24 h (Fig. 2c, d). To investigate the role of ATM activation in G2/M arrest, we co-treated SVN1-67F and SVF1-73F cells with 20 μM of KU-55933 and UVA + 4-OHE$_2$ and found significant reduction in G2/M arrest compared to treatment with UVA + 4-OHE$_2$ in both SVN1-67F (0.7-fold; 30% *vs* 44%) and SVF1-73F (0.6-fold; 31% *vs* 51%) (Fig. 2d).

Cell cycle is tightly controlled by cyclins and cyclin dependent kinase (CDK) enzymes and the progression from G2- to M-phase is driven by activation of the Cdk1/Cyclin B1 complex[48]. We observed an increase in Cyclin B1 levels in SVF1-73F (5-fold, $p < 0.0001$) which was 1.5-fold greater than the increase in SVN1-67F (2-fold, $p < 0.01$) compared to no treatment, confirming a significantly higher G2/M phase arrest in FECD compared to normal cells at 24 h post UVA + 4-OHE$_2$ treatment (Fig. 2e, Supplementary Fig. 10a). Cell cycle arrest has been linked to progression of cellular senescence, a process mediated through the p53-p21 pathway[49]. We next tested for evidence of senescence due to the G2/M phase arrest seen in SVN1-67F and SVF1-73F cells post UVA + 4-OHE$_2$ treatment. While p53/β-actin was elevated in both SVN1-67F normal and SVF1-73F FECD cells, the protein levels of p21/β-actin were greater in SVF1-73F (2.5-fold, $p < 0.01$) compared to SVN1-67F cells (Fig. 2f, Supplementary Fig. 10b). SA-β-Gal staining at 24 h post UVA + 4-OHE$_2$ treatment showed an increase in the percentage of senescent cells in both SVN1-67F and SVF1-7F cells indicating an onset of premature senescence (Fig. 2g).

Loss of NQO1 results in ATM-mediated G2/M phase arrest, leading to upregulation of DNA repair following acute stress with UVA light

NQO1 catalyzes the reduction of reactive quinones to form non-toxic catechol estrogens (4-OHE$_2$). Our previous data demonstrated that loss of NQO1 renders CEnCs highly susceptible to UVA light[44], leading to increased reactive oxygen species (ROS) levels and estrogen genotoxicity,

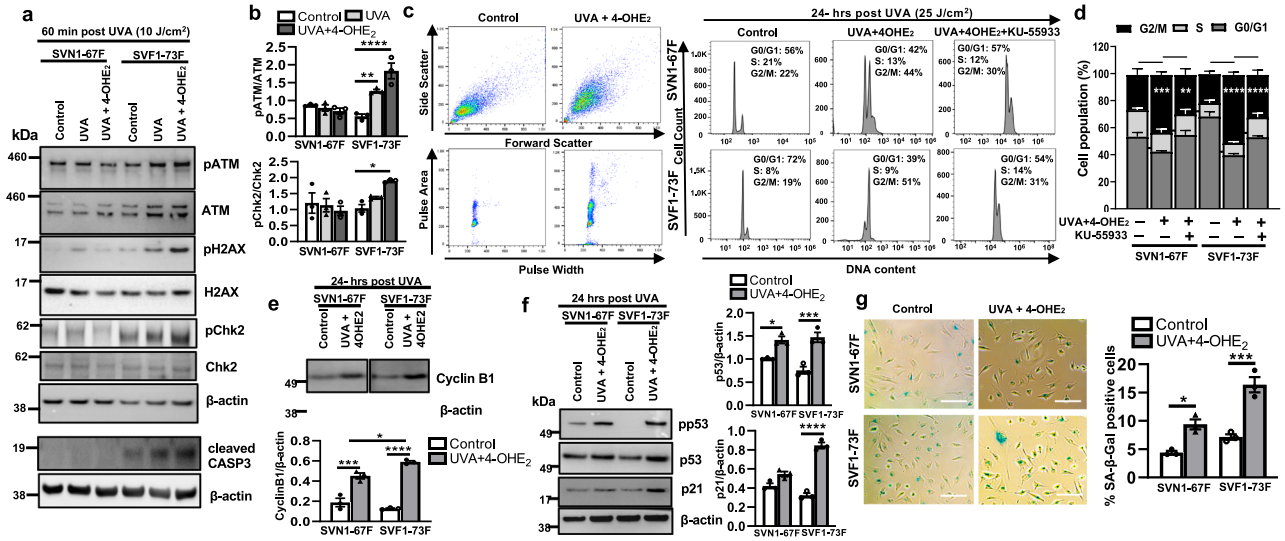

Fig. 2 | Physiological stressors, UVA and 4-OHE$_2$, cause greater ATM-mediated G2/M phase arrest in FECD cells. a Western blot analysis and (**b**) densitometry shows greater activation of phospho-ATM (pATM/ATM) and its downstream effector proteins (pH2AX/H2AX, pChk2/Chk2, CASP3/β-actin) in SVF1-73F compared to SVN1-67F after 60 min of treatment with 10 J/cm^2 UVA (± 10 μM 4-OHE$_2$). **c** Cell cycle analysis by propidium iodide staining and flow cytometry after treatment with UVA + 4-OHE$_2$ demonstrates greater G2/M cell cycle arrest in SVF1-73F compared to normal SVN1-67F cells (center), while this arrest is rescued with 20 μM of ATM inhibitor (KU-55933) (right). **d** Percentage of cells in each stage of the cell cycle. **e** Western blot analysis and densitometry of G2/M marker protein, Cyclin B1, at 24 h post UVA + 4-OHE$_2$ treatment showing greater G2/M arrest in SVF1-73F compared to SVN1-67F cells. **f** Western blot analysis and densitometry of senescence marker proteins, p53/ β-actin and p21/ β-actin, 24 h post UVA + 4-OHE$_2$ treatment shows induction of senescence in SVF1-73F but not SVN1-67F cells. **g** SA-β-GAL staining of control (top) and 24 h post UVA + 4-OHE$_2$ treated (bottom) SVN1-67F and SVF1-73F cells. Data presented as mean values ± SE. Scale bars = 100 μm. ****, ***, **, * indicates $P < 0.0001$, or < 0.001, or < 0.01, or < 0.05 respectively applying one-way ANOVA test with Tukey's Multiple Comparison Test. Data represented as mean ± SEM of N ≥ 3.

thus causing DNA damage and apoptosis[14]. As we detected the UVA-induced G2/M phase cell cycle arrest in FECD CEnCs, we next sought to investigate whether lack of NOQ1, seen in FECD, also exhibits greater ATM activation and G2/M phase arrest. To establish an acute stress cellular model, we utilized our previously generated NQO1-wildtype (*NQO1*$^{+/+}$) and NQO1-null (*NQO1*$^{-/-}$) stable cell lines[10] and exposed them to UVA light (10 J/cm^2 or 25 J/cm^2) and 4-OHE$_2$ (10 μM), with and without ATM inhibitor (KU-55933), and recovered for 60 min or 24 h in low-serum media (Fig. 3a, Supplementary Fig. 11a). Western blot analysis showed greater and significant activation of pATM/ATM and its downstream target pChk2/Chk2 at 60 min after both UVA doses (10 J/cm^2 and 25 J/cm^2) with 4-OHE$_2$, (10 μM) compared to control (Fig. 3b). Next, we examined the effect of greater UVA-mediated ATM activation due to lack of NQO1 on cell cycle progression Cell cycle analysis after treatment with UVA (25 J/cm^2) and 4-OHE$_2$ followed by recovery for 24 h showed an increase in G2/M phase in *NQO1*$^{+/+}$ (2.2-fold; 34% *vs* 15%) and *NQO1*$^{-/-}$ (3.1-fold; 43% *vs* 14%) compared to no treatment (Fig. 3c, d). The cell cycle arrest was further established by increased levels of Cyclin B1 in *NQO1*$^{+/+}$ and *NQO1*$^{-/-}$ cells after UVA + 4-OHE$_2$ exposure as seen by western blotting (Fig. 3d, Supplementary Fig. 11b). We determined that the G2/M arrest was ATM-driven by co-treating cells with KU-55933 and UVA + 4-OHE$_2$ which demonstrated significant reduction in the G2/M phase arrest in both *NQO1*$^{+/+}$ (0.6-fold; 19% *vs* 34%) and *NQO1*$^{-/-}$ (0.5-fold; 20% *vs* 43%) along with a downregulation of Cyclin B1 protein levels compared to no treatment in both cell lines (Fig. 3c, d).

Furthermore, to examine if G2/M arrest under acute stress jumpstarts DNA repair, we sorted both untreated as well as UVA + 4-OHE$_2$ treated *NQO1*$^{+/+}$ and *NQO1*$^{-/-}$ cells from G0/G1 and G2/M phases using cell sorter and extracted the total RNA. Transcription of specific DNA repair genes *LIG3, NEIL2, TOP3A* and *XPC* that are downregulated in FECD ex vivo specimens[50], was quantified for each phase of the cell cycle. None of the 4 DNA repair genes showed a significant difference in expression between G0/G1 and G2/M phases of cell cycle at baseline in *NQO1*$^{+/+}$ or *NQO1*$^{-/-}$ cells (Supplementary Fig. 12). Calculating the ratio of mRNA expression in UVA + 4-OHE$_2$/untreated showed an upregulation in the expression of all 4 DNA repair genes (*LIG3*, *NEIL2, TOP3A* and *XPC*) in G2/M phase of both *NQO1*$^{+/+}$ and *NQO1*$^{-/-}$ cells compared to untreated cells under acute stress (Fig. 3e). Interestingly, this upregulation was significantly greater in G2/M arrested *NQO1*$^{-/-}$ cells - *LIG3* (2.5-fold, $p < 0.01$), *NEIL2* (4-fold, $p < 0.0001$), *TOP3A* (19-fold, $p < 0.0001$), and *XPC* (5-fold, $p < 0.001$) as compared to *NQO1*$^{+/+}$ cells (Fig. 3e). To examine the effect of ATM inhibition on DNA repair in G2/M phase cells, *NQO1*$^{+/+}$ and *NQO1*$^{-/-}$ cells co-treated with KU-55933 and UVA + 4-OHE$_2$ were sorted into G0/G1 and G2/M phases. Gene expression analysis after KU-55933 co-treatment in *NQO1*$^{+/+}$ and *NQO1*$^{-/-}$ cells showed lack of upregulation of DNA repair genes in G2/M phase indicating that ATM-driven G2/M arrest is essential in activating the DNA repair under cytotoxic stress (Fig. 3f). There was no significant change noted in the gene expression of DNA repair genes in the G0/G1 phase of *NQO1*$^{+/+}$ and *NQO1*$^{-/-}$ cells after KU-55933 treatment (Supplementary Fig. 13).

Chronic stress with UVA light leads to a G0/G1 cell cycle arrest, downregulation of DNA repair genes, and cytotoxic senescence, which is reversed by ATM inhibition

Since FECD is a chronic, age-related disorder, that spans many decades for clinical presentation, next we aimed to determine the effect of prolonged (chronic) stress with UVA and 4-OHE$_2$ on ATM-mediated cell cycle arrest, DNA repair, and senescence in *NQO1*$^{+/+}$ and *NQO1*$^{-/-}$ cells. For chronic stress cellular model, *NQO1*$^{+/+}$ and *NQO1*$^{-/-}$ cells were exposed to UVA light (25 J/cm^2) and 4-OHE$_2$ (10 μM), with or without KU-55933 (5 μM) and recovered for 5-days in low-serum medium (Fig. 4a). Chronic stress caused an increase in the G0/G1 phase in both *NQO1*$^{+/+}$ (1.3-fold; 58% *vs* 43%) and *NQO1*$^{-/-}$ (1.4-fold; 64% *vs* 45%) cells, and a decrease in G2/M compared to no treatment (Fig. 4b, c; Supplementary Fig. 14). Addition of KU-55933 reduced G0/G1 phase by 0.8-fold in *NQO1*$^{+/+}$ and 0.6-fold in *NQO1*$^{-/-}$ cells (Fig. 4b, c; Supplementary Fig. 9). G0/G1 arrest was additionally shown by an increase in Cyclin D1 levels which was also reduced after addition of KU-55933 in both *NQO1*$^{+/+}$ and *NQO1*$^{-/-}$ cells, as shown by western blotting (Fig. 4c, Supplementary Fig. 15a).

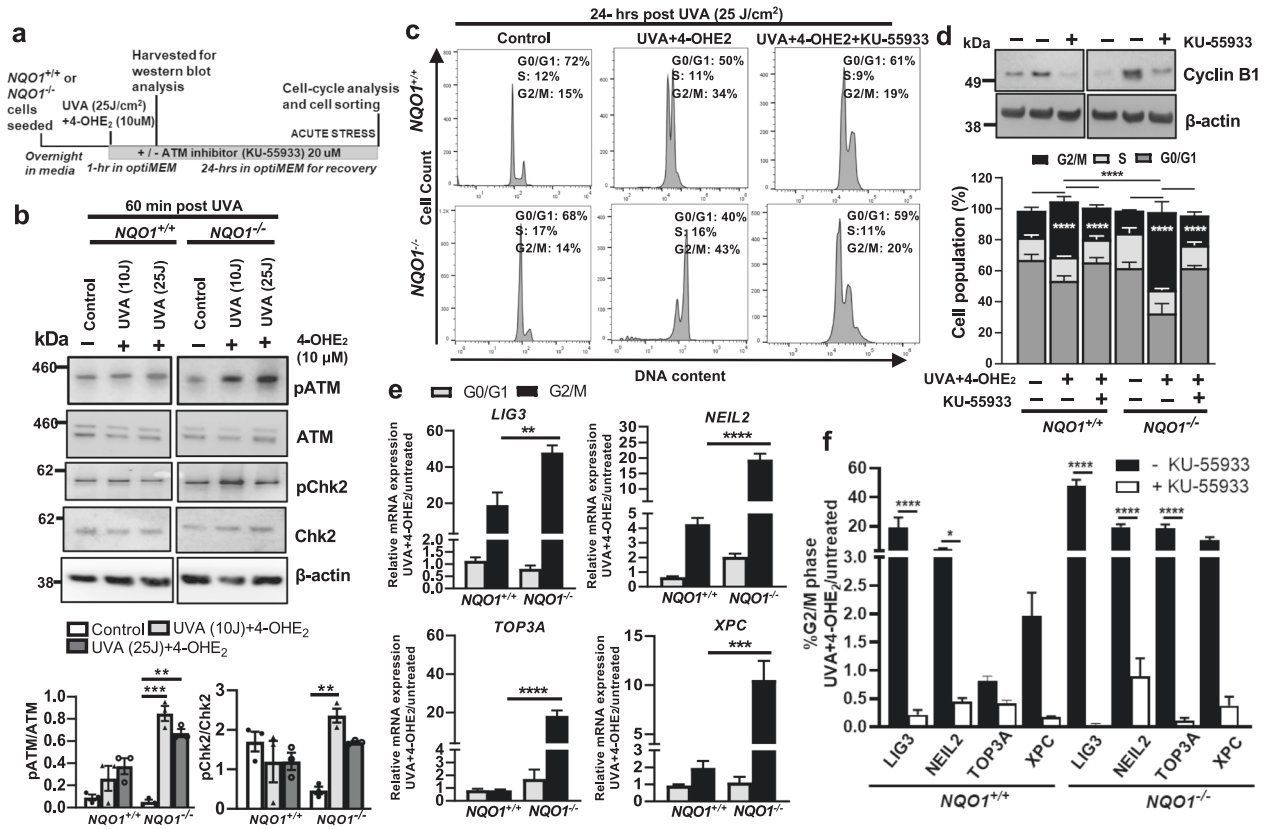

Fig. 3 | Loss of NQO1, as seen in FECD, leads to hyperphosphorylation of ATM and FACS sorting of G2/M arrested NQO1-null cells shows upregulation of DNA-repair genes upon acute UVA + 4-OHE$_2$ treatment. **a** Timeline of acute treatment of NQO1-wildtype (*NQO1*$^{+/+}$) and NQO1-null (*NQO1*$^{-/-}$) cells. **b** Western blot analysis and densitometry showing greater activation of pATM/ATM, and its downstream effector protein, pChk2/Chk2, in *NQO1*$^{-/-}$ compared to *NQO1*$^{+/+}$ cells after 1 hour of treatment with 10 J/cm^2 or 25 J/cm^2 UVA (+ 10 uM 4-OHE$_2$). **c** Cell cycle analysis by propidium iodide staining and flow cytometry after treatment with UVA + 4-OHE$_2$ demonstrating greater G2/M cell cycle arrest in *NQO1*$^{-/-}$ compared to *NQO1*$^{+/+}$ cells (center), while this arrest was rescued with 20 uM of ATM inhibitor (KU-55933) (right). **d** Percentage of cells in each stage of the cell cycle along with western blot of G2/M phase marker protein, cyclin B1, showing the G2/M arrest with UVA + 4-OHE$_2$ and its rescue with addition of 20 uM of ATM inhibitor (KU-55933). **e** Increased mRNA expression of four DNA-repair genes: *LIG3, NEIL2, TOP3A* and *XPC* in G2/M phase of *NQO1*$^{-/-}$ compared *NQO1*$^{+/+}$ cells, displayed as a delta Ct ratio of UVA + 4OHE$_2$/untreated. **f** Reduced mRNA expression of *LIG3, NEIL2, TOP3A* and *XPC* in G2/M phase after treatment with ATM inhibitor (KU-55933) in *NQO1*$^{+/+}$ and *NQO1*$^{-/-}$ cells. ****, ***, **, * indicates $P < 0.0001$, or < 0.001, or < 0.01, or < 0.05 respectively applying one-way ANOVA test with Tukey's Multiple Comparison Test. Data represented as mean ± SEM of N ≥ 3.

To further determine the effect of G0/G1 cell cycle arrest on DNA repair efficiency following chronic stress, we sorted the G0/G1 and G2/M phases of untreated, UVA + 4-OHE$_2$ treated, and UVA + 4-OHE$_2$ + KU-55933 treated *NQO1*$^{+/+}$ and *NQO1*$^{-/-}$ cells and evaluated the expression profiles of four DNA repair genes (*LIG3*, *NEIL2, TOP3A*, and *XPC*) using RT-PCR. Post chronic stress with UVA + 4-OHE$_2$ in *NQO1*$^{+/+}$, the mRNA expression of *LIG3*, *NEIL2*, and *XPC* was predominantly in the G0/G1 phase, albeit significantly lower than that seen in G2/M phase after acute stress (Figs. 4d–g, 3e). Notably, in *NQO1*$^{-/-}$, the expression of *LIG3*, *NEIL2*, and *XPC* was significantly reduced in G0/G1 and G2/M phase cells collectively compared to *NQO1*$^{+/+}$ cells, mimicking end-stage FECD in ex-vivo specimens[50] (Fig. 4d–g). After addition of KU-55933 during the chronic stress, the expression of the DNA repair genes was redistributed between G0/G1 and G2/M in both *NQO1*$^{+/+}$ and *NQO1*$^{-/-}$ cells, with greater expression now noted in the G2/M phase, compared to without KU-55933 treatment (Fig. 4d–g). Remarkably, in *NQO1*$^{-/-}$, after treatment with KU-55933, the expression of *LIG3* and *TOP3A* was found to be significantly greater in both G0/G1 (3- and 7.5-fold) and G2/M (4- and 6-fold) phases, while that of *NEIL2* and *XPC* was significantly greater in G2/M (3.5- and 9.5-fold) phase only, compared to their expression in the respective phases without KU-55933 treatment. This indicates that the observed G0/G1 arrest and diminished DNA repair in *NQO1*$^{-/-}$ cells is indeed ATM-driven and inhibition of ATM forestalls the depletion of DNA repair triggered due to chronic stress.

Chronic stress with UVA + 4-OHE$_2$ also resulted in a greater upregulation of senescence markers *TP53* (p53 protein; 2-fold) and *CDKN1A* (p21 protein; 1.5-fold) in *NQO1*$^{-/-}$ compared to *NQO1*$^{+/+}$ cells indicating greater induction of senescence in a diseased state (Fig. 4h, i). After treatment with KU-55933, the expression of *TP53* and *CDKN1A* was found to be 0.16- and 0.14-fold lower in G0/G1 phase, compared to without KU-55933 treatment in *NQO1*$^{-/-}$ cells (Fig. 4h, i). This was confirmed by western blot showing lower protein level of p53 post UVA + 4-OHE$_2$ and KU-59933 treatment in *NQO1*$^{-/-}$ cells (Fig. 4j, Supplementary Fig. 15b). We also noted a greater positive SA-β-Gal staining following chronic UVA + 4-OHE$_2$ treatment in both *NQO1*$^{+/+}$ and *NQO1*$^{-/-}$ cells, indicating the presence of senescent cells, which was rescued in both cell lines by the addition of KU-55933 (Fig. 4k).

Correlating our findings of how *NQO1*$^{+/+}$ and *NQO1*$^{-/-}$ cells behave under acute *vs* chronic stress with UVA + 4-OHE$_2$ and UVA + 4-OHE$_2$ + KU-55933, we demonstrate that *NQO1*$^{-/-}$ cells (red bold line) exhibit (a) significantly greater (14%) G2/M arrest under acute stress (light grey), and (b) significantly greater (15%) G0/G1 arrest under chronic stress (dark grey), compared to *NQO1*$^{+/+}$ cells (blue bold line). ATM inhibition with KU-55933 under chronic stress restored DNA repair gene expression and reduced senescence, thus favoring cell survival (Fig. 4l). Our study demonstrates that following acute stress, ATM activation results in mild and repairable DNA damage, where cells trigger a series of signaling cascades leading to cell cycle arrest in G2/M, increased turnover of DNA

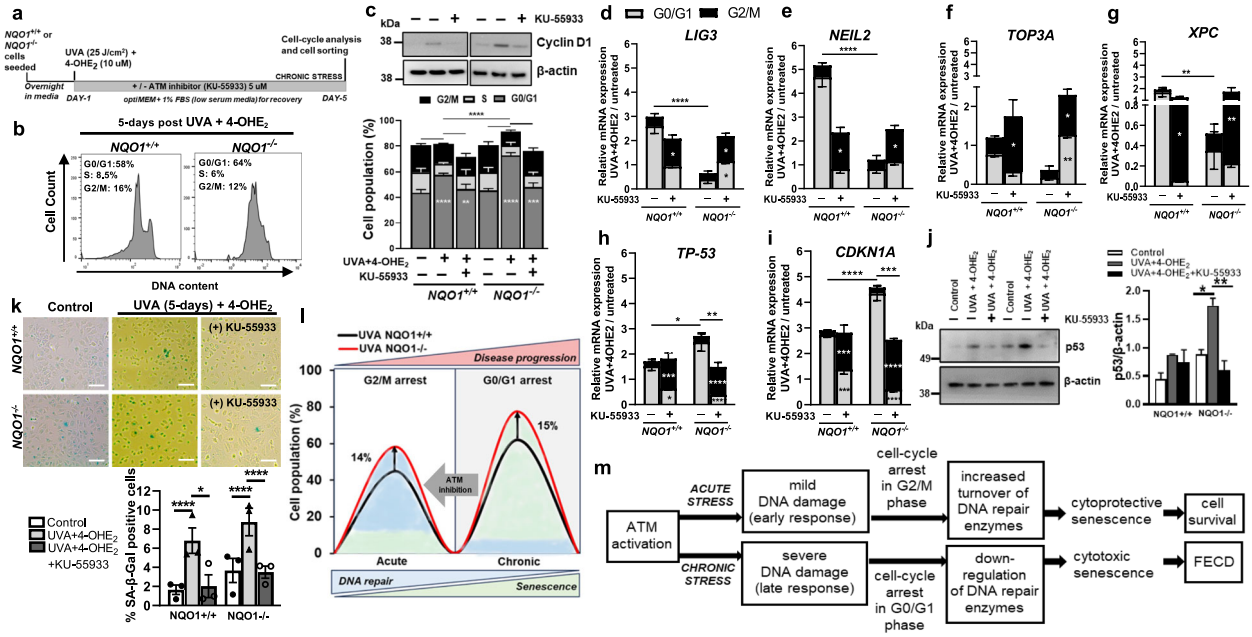

Fig. 4 | Chronic UVA + 4OHE$_2$ treatment in *NQO1*$^{-/-}$ CEnCs demonstrates severe DNA damage, arrest in G0/G1 phase of cell-cycle, and degradation of DNA-repair genes, thus aggravating the induction of cytotoxic senescence. **a** Timeline of chronic treatment of *NQO1*$^{+/+}$ and *NQO1*$^{-/-}$ cells. **b** Cell cycle analysis by propidium iodide staining and flow cytometry after chronic treatment with UVA + 4OHE$_2$ demonstrating greater G0/G1 cell cycle arrest in *NQO1*$^{-/-}$ compared to *NQO1*$^{+/+}$ cells. **c** Percentage of cells in each stage of the cell cycle along with western blot of G0/G1 phase marker protein, cyclin D1, showing the G0/G1 arrest with UVA + 4-OHE$_2$ and its rescue with addition of 5 uM of KU-55933. **d**–**g** Reduced mRNA expression of four DNA-repair genes – *LIG3* (**d**), *NEIL2* (**e**), *TOP3A* (**f**), and *XPC* (**g**) in both G0/G1 and G2/M phases of *NQO1*$^{-/-}$ cells compared *NQO1*$^{+/+}$ cells, displayed as a delta Ct ratio of UVA + 4-OHE$_2$/untreated. Upon treatment with ATM inhibitor (KU-55933) during chronic UVA treatment, differential expression was rescued in G2/M phase for all four genes (*LIG3, NEIL2, TOP3A* and *XPC*), while in G0/G1 phase for only *LIG3* and *TOP3A* in *NQO1*$^{-/-}$ cells. **h**, **i** Increased mRNA expression of *TP53* (**h**), and *CDKN1A* (**i**) genes in G0/G1 phase of *NQO1*$^{-/-}$ cells compared *NQO1*$^{+/+}$ cells, displayed as a delta Ct ratio of UVA + 4-OHE$_2$/untreated. Upon treatment with ATM inhibitor (KU-55933) during chronic UVA treatment, differential expression was rescued in G2/M phase for *TP53* and *CDKN1A* genes, in both *NQO1*$^{+/+}$ and *NQO1*$^{-/-}$ cells. **j** Western blot analysis and densitometry of senescence marker protein p53/ β-actin, 5 days post UVA + 4-OHE$_2$ treatment shows more induction of senescence in *NQO1*$^{-/-}$ cells compared *NQO1*$^{+/+}$ cells. **k** Increased staining (blue) of senescence marker, SA-β-gal, after chronic treatment with UVA + 4OHE$_2$ which was reduced with addition of 20 uM of ATM inhibitor (KU-55933) in *NQO1*$^{+/+}$ and *NQO1*$^{-/-}$ cells. Data presented as mean values ± SE. Scale bars = 50 μm. **l** Graphic representation of differences between acute (light grey) and chronic (dark grey) UVA treatments in *NQO1*$^{+/+}$ (solid black) and *NQO1*$^{-/-}$ (red solid) cells, and rescue with KU-55933 in DNA repair and senescence. **m** Overview of proposed ATM activation pathway under chronic or acute stress conditions in FECD. ****, ***, **, * indicates $P < 0.0001$, or < 0.001, or < 0.01, or < 0.05 respectively applying one-way ANOVA test with Tukey's Multiple Comparison Test. Data represented as mean ± SEM of N ≥ 3.

repair enzymes and premature/cytoprotective senescence, promoting cell survival (Fig. 4m). However, under chronic stress, sustained ATM activation initiates DNA damage cascade leading to cell cycle arrest in G0/G1, downregulation of DNA repair enzymes, and cytotoxic senescence, thus progressing to a diseased state as seen in FECD (Fig. 4m).

UVA-induced cell cycle re-entry, DNA damage, and senescence are reduced in Atm-null mice

To understand the involvement of ATM in the oxidative stress response in vivo, we irradiated the corneas of Atm-wildtype (Atm-WT) and Atm-knockout (Atm-null) mice with 500 J/cm^2 UVA light, a dose that induces FECD phenotype in mice[14]. We evaluated their corneal endothelia visually as well as biochemically at four recovery timepoints, 3 days, 1 week, 2 weeks, and 4 weeks post-UVA (Fig. 5a). The Atm-null mice genotype was determined by PCR analysis (Fig. 5b). Additionally, western blot analyses demonstrated an activation of Atm in Atm-WT mice 1-day post-UVA treatment, which was absent in Atm-null mice (Fig. 5c, Supplementary Fig. 16). The opacity and corneal edema were evaluated in both Atm-WT and Atm-null mice post-UVA using slit lamp bio-microscopy; followed by measurement of central corneal thickness using Anterior Segment Optical Coherence Tomography (AS-OCT) (Supplementary Fig. 17a). An epithelial defect and corneal swelling were observed at day-1 post UVA in both genotypes, as shown in our earlier study[13] (Supplementary Fig. 17a, b). We have previously demonstrated that UVA-induced DNA damage in vivo activates the cell cycle, resulting in G2/M arrest and induction of senescence[45]. To examine the role of DNA damage in cell cycle activation in vivo, we assayed the nuclear expression of Ki67, an indicator of cell cycle re-entry, in the corneas of Atm-WT and Atm-null mice at baseline (no UVA) and at day 2, day 3, and week 1 post-UVA by immunohistochemistry staining (Fig. 5d). At baseline, corneal endothelial cells showed no Ki67 staining in Atm-WT and Atm-null mice. As an immediate response to UVA, both Atm-WT and Atm-null mouse corneal endothelial cells showed 25% Ki67 positivity at day 2 compared to no UVA. However, the Ki67 positivity decreased at day 3 to 11% in Atm-WT and 2.7% in Atm-null and at week 1 to 4.5% in Atm-WT and 2.6% in Atm-null mice compared to day 2 post-UVA. Therefore, the reduction in Ki67 positivity from day 2 to day 3 was 34% greater in Atm-null compared to Atm-WT mice, indicating lower cell cycle activation due to the loss of ATM (Fig. 5d).

Furthermore, we sought to determine the extent of UVA-induced DNA damage by staining for phosphorylated H2AX, a marker of double-strand DNA breaks[51]. Time-dependent increase in DNA damage was detected in Atm-WT mice marked by an increase in percent pH2AX positive nuclei at day 3 (25%), week 1 (35%), week 2 (56%), and week 4 (59%) post-UVA. Atm-null mice presented with a lower pH2AX percent positivity at week 1 (20%), week 2 (20%), and week 4 (44%) compared to Atm-WT mice suggestive of lower DNA damage response in the absence of ATM (Fig. 5e, Supplementary Fig. 18). Next, we checked if UVA-induced cell cycle re-entry and ATM activation progressed to development of senescence detected by increased heterochromatinization, visualized by the presence of tri-methylation of Lys9 on histone H3 (H3K9me3). In Atm-WT

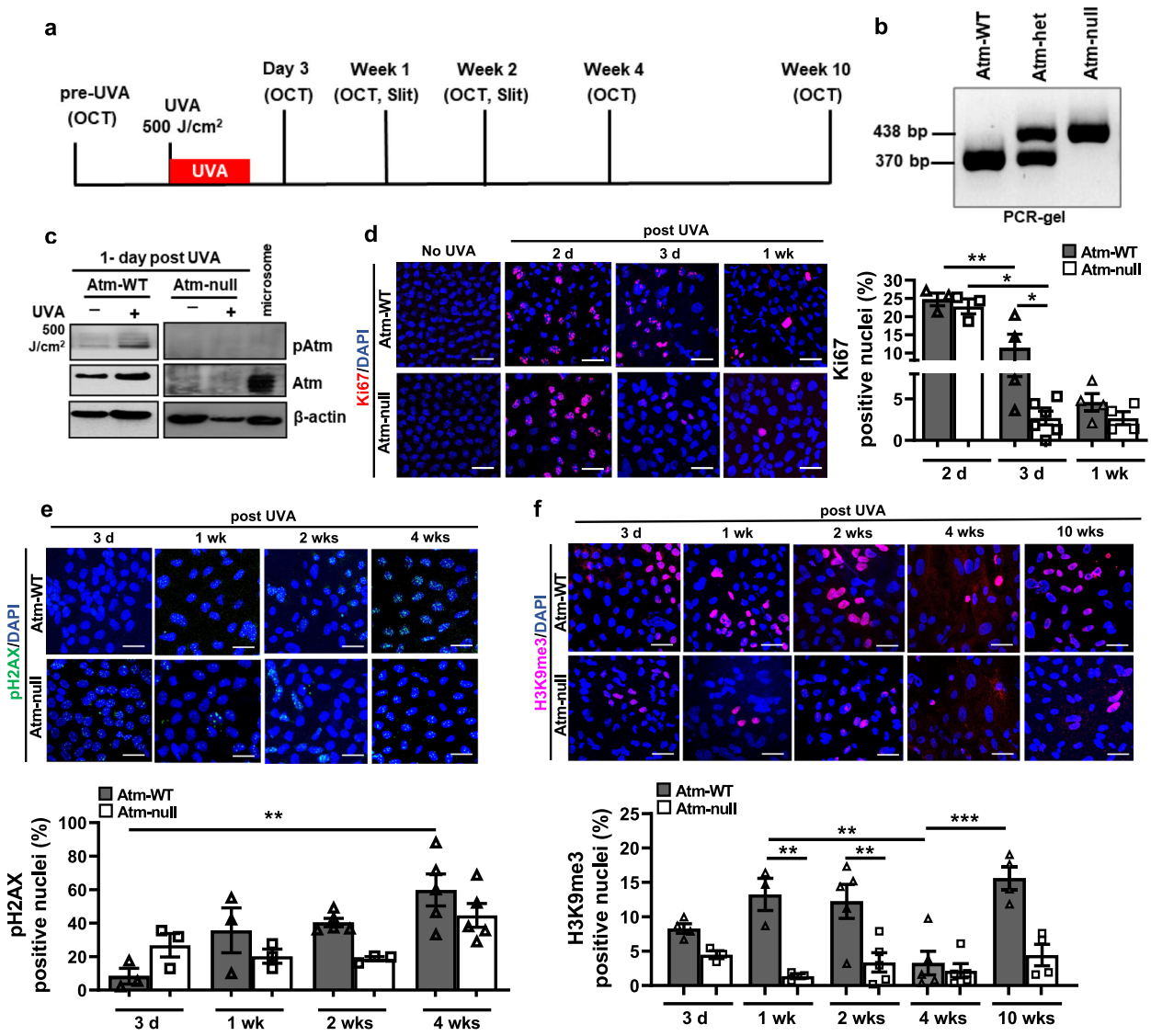

Fig. 5 | UVA-induced cell cycle re-entry, senescence and DNA damage is delayed in the absence of Atm in the mouse model of FECD. a Schematic of the timeline of UVA-irradiation and corneal evaluation by HRT and OCT in Atm-WT and Atm-null mice. **b** Genotyping PCR gel confirming the homozygous knockout of Atm in Atm-null mice. **c** Western blot analysis shows absence of pAtm and Atm proteins in Atm-null mice corneas pre- and one-day post-UVA. β-Actin was used as a loading control and microsome lysate was used as a positive control. **d** Whole mount staining of corneal endothelium with cell cycle re-entry marker Ki67 (red) and DAPI (blue) at baseline (no UVA), 2 days, 3 days and 1-week post-UVA in Atm-WT and Atm-null mice. $^{*}P < 0.05$ applying Unpaired Student's *t*-test. Whole mount staining of the corneal endothelium and quantification of percent (%) positive nuclei for **e** DNA damage marker pH2AX (green foci), and **f** senescence marker H3K9me3 (red), in Atm-WT and Atm-null mice at day 3, week 1, week 2, week 4 and week 10 post-UVA irradiation. ***, * indicates $P < 0.001$, or < 0.05 respectively applying one-way ANOVA test with Tukey's Multiple Comparison Test. Scale bars = 50 µm. Data represented as mean ± SEM of $N \geq 3$.

mice, senescent cells, quantified by calculating percent H3K9me3 positive nuclei, persisted from day 3 (8%) through week 1 (13%), and week 2 (12%), and significantly decreased at week 4 (3%) post-UVA suggesting it to be stress-induced premature senescence[52,53]. In Atm-null mice, senescent cells were significantly lower than Atm-WT at all the tested time-points, day 3 (4%), week 1 (1%), week 2 (3%), and week 4 (2%) post-UVA, indicating that absence of Atm mitigates the onset of senescence (Fig. 5f, Supplementary Fig. 18). Interestingly, at a later time-point of week 10 post UVA, the H3K9me3 positivity was significantly increased in Atm-WT (15%) but not in Atm-null mice (4%), implying that Atm plays a role in the reappearance of prolonged senescence after chronic accumulation of oxidative stress.

Discussion

Cell cycle machinery has been described as a crucial element of DNA damage response (DDR) in post-mitotic cells, like neurons and CEnCs, which either enables repair of damaged DNA or initiates apoptosis upon extensive damage[17]. In neurons, low levels of reactive oxygen species have been shown to promote cell cycle re-entry as opposed to apoptosis, indicating reparable DNA damage facilitates cell cycle re-entry as a survival mechanism to activate DNA repair pathways such as nonhomologous DNA end joining in post mitotic cells[19,54]. While FECD is characterized by the loss of CEnCs due to apoptosis, little is understood about the status of surviving diseased CEnCs and how the disease progresses. We have previously shown increased p53-mediated apoptosis in FECD patient specimens and in vitro cell lines[55]. Also, studies from our lab have demonstrated that UVA irradiation, a physiologically relevant stressor, causes G2/M arrest in vitro in HCEnCs with both senescent and epithelial-mesenchymal transition (EMT) phenotypes detected in G2/M arrested cells[45]. Here, we demonstrate that short-term UVA exposure of diseased CEnCs leads to an early activation of ATM that results in G2/M phase arrest and upregulation of DNA

repair genes. However, during chronic degenerative processes there is an ATM-driven shift to the pro-senescent phenotype that leads to G0/G1 phase arrest and loss of DNA repair capacity. Our findings on ATM-driven cell cycle and DNA repair in FECD underscore the mechanism that could be manipulated to incur cryoprotection based on DDR modulation.

Following DSBs induced by oxidative stress, DNA repair and cell cycle checkpoints are the main mechanisms of maintenance of genomic integrity[56]. Cells have several checkpoints that function at various phases of the cell cycle. Specifically, the G0/G1- and intra-S-phase checkpoints prevent inappropriate DNA replication, whereas the G2/M checkpoint prevents cells with DNA damage from entering mitosis. In the current study, we first detected that increased phosphorylation of ATM plays a central role as an early responder to DSBs in mildly damaged CEnCs due to acute exposure to chemical stressor, menadione. Early hyperactivation of ATM, and not ATR, in FECD cells phosphorylated p53 as the downstream target molecule and resulted in elevated S-phase. The predominant mechanism of S-phase arrest is the inhibition of firing of late origins of replication[57–60]. Onset of DNA repair including repair of inter-strand cross link (ICLs) lesions have been detected during S-phase when encountered by the replication machinery[61,62]. ICLs detected by the replisome initiate a complex set of enzymatic reactions that, with other homologous recombination (HR) events in S-phase, are regulated by Fanconi Anaemia pathway[63]. ATM and other proteins including the MRN complex and BRCA1 have been shown to be required for activation of this checkpoint by activating signaling cascades of ATM-p53-Cdk2-CyclinE and ATM-BRCA1/FANCD2/NBS1/SMC1[64–66].

FECD is a female predominant disorder characterized by an upregulation of genotoxic estrogen metabolites, mainly in the form of catechol estrogens (4-OHE_2) and lack of their neutralization due to loss of NQO1 in the end-stage disease[44,67]. Estrogen metabolites and stress hormone have been shown to activate γH2AX[68,69], resulting in induction of DNA damage. ATM has been previously shown to play a role in suppressing the oncogenic effect of estrogens and preventing estrogen receptor positive breast cancer development[70]. In this study, we detect that both UVA and 4-OHE_2 are activators of DDR, especially ATM, as the major sensor of DSBs. Interestingly, loss of NQO1 leads to hyperactivation of the ATM-driven response as seen in FECD-derived corneal endothelial cells. The hyperactivation of ATM with subsequent Chk2 activation, further upregulated Cyclin B1 leading to G2/M arrest of cell cycle[71], thus preventing cells from undergoing mitosis. As a result, there was marked upregulation of specific base excision repair (BER) genes, that have been shown to be deficient in FECD[50], in the G2/M-sorted $NQO1^{-/-}$ cells as compared to G2/M-sorted $NQO1^{+/+}$ cells after acute stress. This effect, including upregulation of the BER gene levels, was mitigated by ATM inhibitor, KU-55933, after acute stress, indicating that early ATM activation and G2/M cell cycle arrest are critical for jumpstarting the DNA repair process. However, when the cells were exposed to chronic stress, the ensuing persistent DNA damage led to an ATM-driven restriction of cell cycle transition from G1 to S phase, culminating in a G0/G1 arrest, which was significantly more pronounced in $NQO1^{-/-}$ cells. Likewise, the cell cycle-dependent transcriptional analysis of DNA repair genes detected reduction in all four repair genes (*LIG3, NEIL2, TOP3A*, and *XPC*) in the G0/G1 phase of $NQO1^{-/-}$ compared to $NQO1^{+/+}$ cells, notably different from the findings after acute stress. Furthermore, ATM inhibition decreased G0/G1 phase in chronically stressed cells and restored DNA repair back into G2/M phase in both $NQO1^{+/+}$ and $NQO1^{-/-}$ cells, mitigating the effects of sustained DNA damage.

ATM inhibition also decreased the senescence markers in the G0/G1 phase in both cell lines, however, the rescue of senescence was greater in the $NQO1^{-/-}$ cells, indicating the greater effect of ATM in the diseased state. Prolonged cell cycle arrest has been previously described to activate senescence[72] and persistence of DDR is known to initiate this process[73]. Progression to senescence involves cell cycle arrest and the process is mediated through the p53-p21 pathway[74], whose sustained activation has been shown to be sufficient to induce senescence[49,75]. p53-mediated differential transactivation of genes has been shown to help the cell decide between apoptosis or survival[76]. The canonical understanding suggests that senescence predominantly transpires in the G1 or sometimes in the G2 phases of the cell cycle, with quiescence prevailing in the G0 phase[77]. Under acute stress conditions, we detected a transient cell cycle arrest in G2/M that triggered the initial activation of p53-p21 initiating premature senescence as a cytoprotective mechanism. However, our chronic cellular FECD model induced a substantial DNA damage response, upregulating the p53 (*TP53* gene) and p21 (*CDKNA1* gene) pathway and transitioning the cells to the state of mature cytotoxic senescence. Remarkably, inhibition of ATM by use of KU-55933 inhibitor attenuated senescence in our chronic cellular FECD model *via* reduction in SA-β-Gal positivity[78].

We have previously shown that UVA-irradiation of wildtype mouse corneal endothelial cells in vivo induces cell cycle reentry to G2/M phase and progress to senescence[45]. Similar cell-cycle re-entry has also been described in other post-mitotic cells like neurons which contribute to mild cognitive impairment and early Alzheimer's disease pathology, as well as other neurodegenerative diseases[79–81]. In corroboration with our in vitro findings, we noted that in vivo, UVA irradiation activates the cell cycle and increases Ki67 expression in response to DNA damage, in the post-mitotic cells of the ocular tissue. However, the cell cycle activation gradually diminished with time, with a faster decrease in Ki67 positivity in Atm-null mice (at day 3) compared to Atm-WT (at week 1). Furthermore, Atm-WT, but not Atm-null mice, showed a greater increase in H3K9me3 positivity at weeks-1 and 2 and then again at week 10 post-UVA, suggesting the onset of both premature senescence and cytotoxic senescence in the presence of functional ATM. Our data shows that G2/M checkpoint plays a pivotal role in regulating the effects of DNA damage in normally quiescent CEnCs after UVA exposure, as seen in FECD degeneration.

Interestingly, UVA exposure also triggered substantially greater pH2AX foci formation in Atm-WT compared to Atm-null mouse CE. Likewise, a previously published study has demonstrated that H2AX phosphorylation is significantly reduced in Atm−/− compared to WT mouse embryonic fibroblasts, indicating that ATM is the major DDR kinase involved in phosphorylation of H2AX and is one of the earliest kinases to be activated in the cellular response to double strand breaks[31]. The presence of fewer and enlarged nuclei at week 4 after UVA exposure in both Atm-WT and Atm-null suggests that the cells may have undergone a mitotic defect, possibly failed cytokinesis which may result in the development of polyploidy[82].

Targeting ATM, the master regulator of the DDR, has demonstrated neuroprotective effects. Caffeine, a nonspecific inhibitor of ATM and other phosphatidylinositol 3-kinase family members, protects against etoposide-induced DNA damage and cell death in neurons in vitro, and genetic reduction of ATM gene dosage is neuroprotective in mouse models of Huntington's disease[83,84]. Recent studies have demonstrated that targeting the central ATM-Chk2 pathway which regulates the double-strand breaks, slows down neural decline in Drosophila models of chronic neurodegeneration[85]. Administration of clinically relevant Atm-Chk2 inhibitors to rats, following spinal cord and optic nerve injury, is shown to result in significant axon regeneration/sprouting and a marked recovery of lost sensory, motor, and visual function[85]. Additionally, since ATM hyper-activation during oxidative stress promotes photoreceptor cell death in progressive retinitis pigmentosa and age-related macular degeneration[86], loss of ATM and 53BP1 in mice photoreceptors has been shown to lower the activation of cell death signaling in post-mitotic neurons[87]. Recently, it was also reported that terminally differentiated and post-mitotic osteoclast cells show better survival in the absence of ATM[88].

In this study, we demonstrate that the effects of acute and chronic oxidative stress-induced cell cycle arrest and DNA repair are ATM-driven by using ATM inhibitor – KU-55933 in our in-vitro FECD cellular models. KU-55933 is the first potent and selective ATM inhibitor that has been demonstrated to confer sensitization to IR and DNA DSB-inducing chemotherapeutics[46]. Importantly, in cells derived from ataxia-telangiectasia patients, which express no functional ATM, no radiosensitization was observed, validating the selectivity of KU-55399 compound towards ATM[46]. In the presence of DSB, KU-55933 has been shown to significantly block HR repair signals by γ-H2AX and RAD51 focal

reduction in human melanoma cells[89]. Although this compound is commonly used as an ATM kinase inhibitor, it has been described to have limited utility in vivo owing to its high lipophilicity[90]. In our study, co-treatment of KU-55933 with UVA and 4-OHE_2 in acute cellular FECD model showed an abrogation of the observed upregulation of DNA repair genes in G2/M phase cells, thus signifying the role of ATM as a key regulator of this process. However, in our chronic cellular FECD model, co-treatment of KU-55933 with UVA and 4-OHE_2, displayed a protective mechanism which averted the G0/G1 phase arrest and restored the expression of DNA repair genes in the G2/M phase. This indicates that chronic ATM activation renders the cells prone to accumulation of DNA damage due to deficient DNA repair during the G0/G1 phase arrest.

Our data reveals that ATM is not only a key activator of DDR in CEnCs due to oxidative stress, but also a master controller of cell cycle progression, transcriptional regulation of DNA repair genes, and senescence. The in vitro UVA FECD models used in this study highlight the potential of ATM inhibition in delaying DDR, promoting cell cycle progression, restoring DNA repair processes, and forestalling senescence in diseased CEnCs. Senescent cells are known to secrete many factors such as cytokines, growth factors, matrix remodeling proteins, proteases, and chemokines, which are collectively referred to as the senescence-associated secretory phenotype (SASP)[91]. The most prominent component of SASP is interleukin-6 (IL-6), a pleiotropic pro-inflammatory cytokine whose secretion is shown to increase due to DDR-dependent senescence in a variety of cell types[92–94]. Interestingly, inhibition of ATM is shown to prevent IL-6 from contributing to the proliferation of glioblastoma cells after IR[95]. Based on our study, and those of others, ATM inhibition could also be efficacious in the setting of diseases like FECD involving oxidative stress and pro-inflammatory cytokine signaling. In the future, inhibition of ATM after its early activation along with specific cell cycle checkpoints may be an effective combinatorial therapy to improve corneal function by enhancing DNA repair and delaying senescence. In summary, this study provides insights into understanding the role of ATM activation in DDR signaling cascade and regulation of cell cycle in FECD. Based on our findings herein, we suggest that ATM-driven modulation of the cell cycle and DNA repair can potentially provide an effective therapeutic strategy against FECD.

Methods

Cell culture

Corneal endothelial cell lines were derived from Descemet's membrane and endothelium collected from either a normal cadaveric donor (67 year-old female with 15/16 CTG repeats - SVN1-67F) or FECD patients that underwent endothelial keratoplasty (73 year-old female with 16/74 CTG repeats - SVF1-73F and 54 year-old female with 11/73 CTG repeats - SVF5-54F) by immortalization using SV40 T Antigen Cell Immortalization Kit (#CILV01, Alstem Cell Advancements, Richmond, CA) as described previously[12,96]. *NQO1*$^{+/+}$ and *NQO1*$^{-/-}$ cells were generated from normal HCEnC-21T cell line (derived from a 21-year-old normal male cadaveric donor) using the CRISPR-Cas9 system as previously reported[10]. Cells were cultured in Chen's medium containing OptiMEM-I (#51985091, Life Technologies), 8% fetal bovine serum (#10082147, Life Technologies), 5 ng/mL epidermal growth factor (#01-101, Millipore), 66 µg/mL bovine pituitary extract (#500-102, Gemini Bioproducts), 200 mg/L calcium chloride (#C7902, Sigma-Aldrich), 0.08% chondroitin sulfate (#C9819, Sigma-Aldrich), 50 mg/mL gentamicin (#15750078, Life Technologies), and 1:100 diluted antibiotic/antimycotic solution (#15240062, Life Technologies). Sub-culturing of CEnCs was performed using 0.05% Trypsin (#25300120, Life Technologies) for 5 min at 37°C.

In vitro acute treatment with Menadione

For treatments with menadione (MN), MN powder (#M5750, Sigma) was freshly dissolved in sterile distilled water to make a 10 mM working stock. Cells were seeded in complete Chen's medium at a density of 0.35 × 10^6 cells on FNC (#0407, Athena ES)-coated 6-well plates overnight at 37 °C with 5% CO_2. To assay the levels of DDR proteins, cells were incubated with 25 µM MN diluted in serum-free DMEM (#10567014, Life Technologies) followed by harvesting after 30, 60, 90, or 120 min for western blotting. For ATM inhibitor treatment, 20 µM KU-55933 (#118500, Calbiochem) was used to pre-treat cells for 30 min in Chen's medium, then co-treat with MN in DMEM, and then was added to OptiMEM-I during the 24 h recovery period. To determine the cell cycle fate after MN stress, cells were treated with 50 µM MN for 60 min in DMEM followed by a 24 h recovery period in OptiMEM-I and then harvested for flow cytometry analysis.

In vitro acute treatment with UVA light and 4-OHE_2

For acute treatments with ultraviolet-A light plus 4-hydroxyestradiol (UVA + 4-OHE_2), 0.4 × 10^5 cells were seeded in estrogen-free Chen's medium (modifications-phenol red-free OptiMEM (#11058021, Life Technologies) and 8% charcoal-stripped fetal bovine serum (FBS) (#100-119, Gemini Bio-products) on FNC-coated 6-well plates overnight. For UVA irradiation, growth medium was replaced with sterile phosphate buffered saline (PBS) and cells were exposed to two 19.5-inch UVA tubes (XX-15L; Analytik Jena US LLC) emitting 365 nm light (irradiance: 14.77 mW/cm^2) to deliver a fluence of either 10 J/cm^2 (11 minutes) or 25 J/cm^2 (27 minutes), followed by a 24 h recovery period in phenol red-free OptiMEM. For 4-OHE_2 treatments, 4-OHE_2 powder (#E2500-000, Steraloids) was dissolved in 100% ethanol to make a 50 mM master stock which was freshly diluted in sterile PBS and added to cells immediately after UVA irradiation at 10 µM concentration in phenol red-free OptiMEM. For ATM inhibitor treatment, cells were pre-treated with 20 µM KU-55933 for 30 min in estrogen-free Chen's medium and then re-added to cells in phenol red-free OptiMEM immediately after UVA irradiation. To assay the levels of DDR proteins, cells were harvested at 1 h post UVA or UVA + 4-OHE_2 treatments for western blotting. To determine the cell cycle fate, cells were harvested 24 h post UVA + 4-OHE_2 with or without KU-55933 treatment for cell cycle analysis and cell sorting by flow cytometry (Fig. 3a).

In vitro chronic treatment with UVA light and 4-OHE_2

For chronic UVA + 4-OHE_2 treatments, 0.1 × 10^5 cells were seeded in estrogen-free Chen's medium on FNC-coated 6-well plates overnight. Cells were pre-treated with 5 µM KU-55933 for 30 min and then exposed to 25 J/cm^2 UVA followed by addition of 10 µM 4-OHE_2 with or without re-addition of 5 µM KU-55933 as described above. Media was replaced with fresh phenol red-free OptiMEM every 48 h and cells were harvested for cell cycle analysis and cell sorting by flow cytometry on day 5 (Fig. 4a).

Immunoprecipitation and Western blotting

Whole cell lysates were prepared by lysis in RIPA buffer containing HALT protease and phosphatase inhibitors (#78440, Life Technologies) for 30 min on ice. Protein concentration was determined using the BCA assay kit (#23225, Life Technologies). For immunoprecipitation, cells were lysed in immunoprecipitation lysis buffer for 15 min and centrifuged at 14000 rpm for 10 min at 4 °C. Total protein concentration was determined as described above. Protein samples were first precleared with protein A or G beads for 30 min and then incubated with 2 µg anti-pATM antibody (#05-740, Millipore) for 2 h at 4 °C followed by the addition of 35 µl of protein A- or G-sepharose slurry and rotating for 1 h. Protein A/G beads were collected and washed with lysis buffer four times. Immunoprecipitates or whole cell lysates were resolved by loading onto a 4–12% Bis-Tris gel for SDS-PAGE and blotted onto a polyvinylidene difluoride membrane (#IPVH00010, Millipore) which was blocked in 5% nonfat milk (#1706404, Bio-Rad) or 5% bovine serum albumin (#BP1600, Fisher Scientific) in tris-buffered saline with 0.1% Tween-20 (TBST) for 1 h and incubated overnight with primary antibody at 4°C. (Refer Supplementary table 1 for list of primary antibodies used). Blots were exposed to HRP-conjugated anti-mouse (#sc-516102) or –rabbit IgG (#sc-2357) from Santa Cruz Biotechnology Inc., USA for 1 h. The membrane was developed with SuperSignal West Pico or Femto (#34577 or # 34096, Life Technologies, USA) plus chemiluminescent substrate. Densitometry was analyzed with ImageJ software (developed by Wayne Rasband, National Institutes of Health, Bethesda, MD), and protein

content was normalized relative to β-actin protein content. Experiments were repeated a minimum of three times. Results were averaged and SEM values were calculated.

Cellular viability and morphology

Phase-contrast microscopy (Leica DM IL LED) was employed to visualize cell morphology. Cell Titer Glo reagent (#G9241, Promega, Madison, WI) was used to determine the cell viability, according to the manufacturer's protocol. The luminescence was determined by a luminometer (Turner Biosystems, Sunnyvale, CA).

Cell cycle analysis and cell sorting

Cell cycle analysis and cell sorting were performed as previously published[45]. Briefly, CEnCs were fixed with 70% ethanol for 20 min, treated with 100 µg/ml RNase, and stained with 50 µg/ml propidium iodide. Cell cycle data was acquired using a BD LSR II flow cytometer. Single cells were identified by measuring forward and side scatter, and cell doublets were excluded. The combined gates were applied to a forward scatter *versus* propidium iodide signal (PE channel) to produce a histogram plot. Quantification of cells in each phase of the cell cycle was carried out using FlowJo cell cycle analysis (v10.6.2, FlowJo, LLC). For FACS (Fluorescence-Activated Cell Sorting), G0/G1 and G2/M phase cells were sorted and collected in PBS, using Cytomation MoFlo cell sorter and resuspended in Trizol (Invitrogen) for RT-PCR analysis.

RT-PCR

RNA was extracted from cultured CEnCs using Trizol (Invitrogen) and RNeasy Micro Kit (Qiagen, Valencia, CA) according to manufacturer's protocol. RNA quality and quantity were measured using NanoDrop spectrophotometer (Life Technologies). iScript cDNA synthesis kit (Bio-Rad, Hercules, CA) was used to reverse-transcribe RNA. RT-PCR was performed by TaqMan gene expression assays (Applied Biosystems, Foster City, CA) with 2X Kapa Probe Fast master mix (#KK4703, Roche) for detection of mRNA expression of all genes. Results were normalized to GAPDH internal control and relative expression expressed as $2^{\wedge-\Delta\Delta(CT)}$. The TaqMan assays used for RT-PCR are listed in Supplementary Table 2.

SA-β-GAL staining

Cell lines were stained for SA-β-GAL using a senescence histochemical staining kit (#CS0030, Sigma-Aldrich) according to the manufacturer's protocol, with an incubation period of 16 h at 37 °C. Images of stained cells (10 images acquired at ×20 magnification for each well) were captured using bright field microscopy (EVOS XL Core). For quantification, positively stained cells were manually counted and reported as a percentage of total cells.

Atm-wild type and -null mice

Wildtype $Atm^{tm1Mmpl+/+}$ (Atm-WT), heterozygous $Atm^{tm1Mmpl/+}$ (Atm-het), and knockout $Atm^{tm1Mmpl/tm1Mmpl}$ (Atm-null) were provided as a kind gift by Dr. Margot Mayer-Proschel, University of Rochester Medical Center, New York[97]. The strain was maintained by setting up monogamous pairs consisting of one male and one female mouse crossed as per a heterozygous X heterozygous breeding scheme and the litters were genotyped by PCR to identify knockouts and wildtypes for the experiments. Mice were housed at Schepens Eye Research Institute, Boston, USA, in a controlled environment with constant temperature, 12 h light/dark cycle, and food and water available ad libitum. Mice were anesthetized with a combined dose of ketamine (100 mg/kg) and xylazine (20 mg/kg) administered intraperitoneally (IP). Animal studies were in accordance with the ARVO Statement for the Use of Animals in Ophthalmic and Visual Research as well as the NIH Guide for the Care and Use of Animals and were performed at Schepens Eye Research Institute (SERI) with approval from SERI Institutional Animal Care and Use Committees IACUC.

UVA Irradiation of Mouse Cornea and in vivo imaging

UVA irradiation of the mouse corneas was performed as described in our earlier publication[13]. Briefly, a UVA LED source (M365LP1; Thorlabs, USA) with an emission peak of 365 nm light, 8 nm bandwidth (FWHM), and irradiance of 398 mW/cm^2 was focused down to a 4 mm diameter illumination spot onto the mouse cornea. The time of UVA exposure was adjusted to deliver the appropriate fluence (20 minutes 57 s for 500 J/cm^2) as measured with a thermal power sensor head (S425C, Thorlabs, USA) and energy meter console (PM100D, Thorlabs). The right eye (OD) was irradiated, while the contralateral eye (OS) was covered with retention drapes (SpaceDrapes, Inc., USA) and served as untreated control eye). Mouse eyes were enucleated in sterile PBS, and corneal were isolated, snap-frozen, and sent for estrogen metabolite analysis or western blot following treatment with vehicle or drugs. For in vivo imaging, mice were anesthetized as described earlier, and visual assessment of their corneas was performed as described in our prior publication[14] pre-UVA and 1 day, 3 days, 1 week, 2 weeks, and 4 weeks post-UVA. Briefly, a slit lamp biomicroscope attached to a camera (SL-D4, Topcon Healthcare, The Netherlands) was used to assess the epithelial cell integrity. Anterior segment images were taken using anterior segment optical coherence tomography (OCT) (Bioptigen Spectral Domain Ophthalmic Imaging System Envisu R2200) with a 12 mm telecentric lens to scan the cornea and measure central corneal thickness.

Immunohistochemistry

Mouse eyes were enucleated either at day 1, day 3, week 1, week 2, week 4, or week 10 post irradiation in sterile, ice-cold PBS. Under a stereo-zoom microscope (MZ6, Leica), the eyeball was penetrated with a 26-gauge syringe needle to create an incision at the corneo-scleral junction. Curved Vannas capsulotomy scissors, 3 3/8" (5677E, Ambler Surgical) were inserted into the incision to snip out the corneal cup from which the lens was removed, and remaining iris and loose tissue was scraped. The corneal cups were fixed in 4% paraformaldehyde (PF) for 20 min at room temperature (RT). For H3K9me3 and Ki67 staining, the corneal cup was permeabilized and blocked in 3% BSA + 0.1% TX-100 + 1% donkey serum in PBS for 1 h at RT with gentle shaking followed by an additional 10 min of blocking in 10% donkey serum. For Ki67, an additional permeabilization step with 1% TX-100 for 10 min was applied prior to blocking. The corneal cups were incubated with primary antibodies at 4 °C overnight and with rhodamine conjugated donkey anti-rabbit secondary antibody next day for 1 h at RT. For pH2AX staining, the corneal cups were permeabilized in 0.1% Triton X100 + 3% BSA in PBS for 30 min at RT with gentle shaking, followed by incubation with primary antibody at 4°C overnight and then with Fluorescein Isothiocyanate (FITC) conjugated goat anti-mouse antibody next day for 1 h at RT. (Refer Supplementary table 1 for list of antibodies used). The tissues were incubated with DAPI dye, mounted onto glass slides with Antifade mounting medium (#H-1000-10, Vector Labs) and imaged on Leica SP8.

Statistical analysis

Statistical analysis was carried out using GraphPad Prism V10 (GraphPad Software Inc, CA) using Student's *t*-test for comparing two groups and one- or two-way analysis of variance (ANOVA) with Tukey's post hoc test for comparing 3 or more groups. All data is reported as the mean ± SEM. Significance for all measures was set at $P < 0.05$.

Reporting summary

Further information on research design is available in the Nature Portfolio Reporting Summary linked to this article.

Data availability

The data generated during and/or analyzed during the current study is archived to Mass General Brigham (MGB) Dropbox with unlimited storage. The data is available upon request from the corresponding author.

Received: 2 May 2024; Accepted: 31 October 2024;
Published online: 10 November 2024

References

1. Jurkunas, U. V. Fuchs Endothelial Corneal Dystrophy Through the Prism of Oxidative Stress. *Cornea* **37**, S50–S54 (2018).
2. Schmedt, T. et al. Telomerase immortalization of human corneal endothelial cells yields functional hexagonal monolayers. *PLoS One* **7**, e51427 (2012).
3. Mimura, T. & Joyce, N. C. Replication competence and senescence in central and peripheral human corneal endothelium. *Invest Ophthalmol. Vis. Sci.* **47**, 1387–1396 (2006).
4. Joyce, N. C., Zhu, C. C. & Harris, D. L. Relationship among oxidative stress, DNA damage, and proliferative capacity in human corneal endothelium. *Invest Ophthalmol. Vis. Sci.* **50**, 2116–2122 (2009).
5. Matthaei, M. et al. Fuchs Endothelial Corneal Dystrophy: Clinical, Genetic, Pathophysiologic, and Therapeutic Aspects. *Annu Rev. Vis. Sci.* **5**, 151–175 (2019).
6. Krachmer, J. H., Purcell, J. J. Jr., Young, C. W. & Bucher, K. D. Corneal endothelial dystrophy. A study of 64 families. *Arch. Ophthalmol.* **96**, 2036–2039 (1978).
7. Rosenblum, P., Stark, W. J., Maumenee, I. H., Hirst, L. W. & Maumenee, A. E. Hereditary Fuchs' Dystrophy. *Am. J. Ophthalmol.* **90**, 455–462 (1980).
8. Bahn, C. F. et al. Classification of corneal endothelial disorders based on neural crest origin. *Ophthalmology* **91**, 558–563 (1984).
9. Halilovic, A. et al. Menadione-Induced DNA Damage Leads to Mitochondrial Dysfunction and Fragmentation During Rosette Formation in Fuchs Endothelial Corneal Dystrophy. *Antioxid. Redox Signal* **24**, 1072–1083 (2016).
10. Katikireddy, K. R. et al. NQO1 downregulation potentiates menadione-induced endothelial-mesenchymal transition during rosette formation in Fuchs endothelial corneal dystrophy. *Free Radic. Biol. Med.* **116**, 19–30 (2018).
11. Jurkunas, U. V., Bitar, M. S., Funaki, T. & Azizi, B. Evidence of oxidative stress in the pathogenesis of fuchs endothelial corneal dystrophy. *Am. J. Pathol.* **177**, 2278–2289 (2010).
12. Ong Tone, S. et al. Increased Corneal Endothelial Cell Migration in Fuchs Endothelial Corneal Dystrophy: A Live Cell Imaging Study. *Ophthalmol. Sci.* **1**, 100006 (2021).
13. Liu, C. et al. Ultraviolet A light induces DNA damage and estrogen-DNA adducts in Fuchs endothelial corneal dystrophy causing females to be more affected. *Proc. Natl Acad. Sci. USA* **117**, 573–583 (2020).
14. Kumar, V. et al. Estrogen genotoxicity causes preferential development of Fuchs endothelial corneal dystrophy in females. *Redox Biol.* **69**, 102986 (2024).
15. Hamilton, M. L. et al. Does oxidative damage to DNA increase with age? *Proc. Natl Acad. Sci. USA* **98**, 10469–10474 (2001).
16. Zhou, B. B. & Elledge, S. J. The DNA damage response: putting checkpoints in perspective. *Nature* **408**, 433–439 (2000).
17. Kruman, I. I. et al. Cell cycle activation linked to neuronal cell death initiated by DNA damage. *Neuron* **41**, 549–561 (2004).
18. Fortini, P. & Dogliotti, E. Mechanisms of dealing with DNA damage in terminally differentiated cells. *Mutat. Res.* **685**, 38–44 (2010).
19. Schwartz, E. I. et al. Cell cycle activation in postmitotic neurons is essential for DNA repair. *Cell Cycle* **6**, 318–329 (2007).
20. Vendetti, F. P. et al. Pharmacologic ATM but not ATR kinase inhibition abrogates p21-dependent G1 arrest and promotes gastrointestinal syndrome after total body irradiation. *Sci. Rep.* **7**, 41892 (2017).
21. Aird, K. M. et al. ATM couples replication stress and metabolic reprogramming during cellular senescence. *Cell Rep.* **11**, 893–901 (2015).
22. Stuart, A. & de Lange, T. Replicative senescence is ATM driven, reversible, and accelerated by hyperactivation of ATM at normoxia. *bioRxiv*. https://doi.org/10.1101/2024.06.24.600514 (2024).
23. van Gent, D. C., Hoeijmakers, J. H. & Kanaar, R. Chromosomal stability and the DNA double-stranded break connection. *Nat. Rev. Genet* **2**, 196–206 (2001).
24. Khanna, K. K., Lavin, M. F., Jackson, S. P. & Mulhern, T. D. ATM, a central controller of cellular responses to DNA damage. *Cell Death Differ.* **8**, 1052–1065 (2001).
25. Paull, T. T. Mechanisms of ATM Activation. *Annu Rev. Biochem.* **84**, 711–738 (2015).
26. Bakkenist, C. J. & Kastan, M. B. DNA damage activates ATM through intermolecular autophosphorylation and dimer dissociation. *Nature* **421**, 499–506 (2003).
27. Kozlov, S. V. et al. Involvement of novel autophosphorylation sites in ATM activation. *EMBO J.* **25**, 3504–3514 (2006).
28. Sun, Y., Xu, Y., Roy, K. & Price, B. D. DNA damage-induced acetylation of lysine 3016 of ATM activates ATM kinase activity. *Mol. Cell Biol.* **27**, 8502–8509 (2007).
29. Lee, J. H. & Paull, T. T. ATM activation by DNA double-strand breaks through the Mre11-Rad50-Nbs1 complex. *Science* **308**, 551–554 (2005).
30. Stracker, T. H. & Petrini, J. H. The MRE11 complex: starting from the ends. *Nat. Rev. Mol. Cell Biol.* **12**, 90–103 (2011).
31. Burma, S., Chen, B. P., Murphy, M., Kurimasa, A. & Chen, D. J. ATM phosphorylates histone H2AX in response to DNA double-strand breaks. *J. Biol. Chem.* **276**, 42462–42467 (2001).
32. Savic, V. et al. Formation of dynamic gamma-H2AX domains along broken DNA strands is distinctly regulated by ATM and MDC1 and dependent upon H2AX densities in chromatin. *Mol. Cell* **34**, 298–310 (2009).
33. Banin, S. et al. Enhanced phosphorylation of p53 by ATM in response to DNA damage. *Science* **281**, 1674–1677 (1998).
34. Chehab, N. H., Malikzay, A., Stavridi, E. S. & Halazonetis, T. D. Phosphorylation of Ser-20 mediates stabilization of human p53 in response to DNA damage. *Proc. Natl Acad. Sci. USA* **96**, 13777–13782 (1999).
35. Marine, J. C. & Lozano, G. Mdm2-mediated ubiquitylation: p53 and beyond. *Cell Death Differ.* **17**, 93–102 (2010).
36. Sullivan, K. D., Gallant-Behm, C. L., Henry, R. E., Fraikin, J. L. & Espinosa, J. M. The p53 circuit board. *Biochim Biophys. Acta* **1825**, 229–244 (2012).
37. Lane, D. P. Exploiting the p53 pathway for cancer diagnosis and therapy. *Br. J. Cancer* **80**, 1–5 (1999).
38. Houldsworth, J. & Lavin, M. F. Effect of ionizing radiation on DNA synthesis in ataxia telangiectasia cells. *Nucleic Acids Res.* **8**, 3709–3720 (1980).
39. Falck, J., Mailand, N., Syljuasen, R. G., Bartek, J. & Lukas, J. The ATM-Chk2-Cdc25A checkpoint pathway guards against radioresistant DNA synthesis. *Nature* **410**, 842–847 (2001).
40. Bennetzen, M. V. et al. Site-specific phosphorylation dynamics of the nuclear proteome during the DNA damage response. *Mol. Cell Proteom.* **9**, 1314–1323 (2010).
41. Bensimon, A. et al. ATM-dependent and -independent dynamics of the nuclear phosphoproteome after DNA damage. *Sci. Signal* **3**, rs3 (2010).
42. Xu, Y. et al. Targeted disruption of ATM leads to growth retardation, chromosomal fragmentation during meiosis, immune defects, and thymic lymphoma. *Genes Dev.* **10**, 2411–2422 (1996).
43. Guo, Z., Kozlov, S., Lavin, M. F., Person, M. D. & Paull, T. T. ATM activation by oxidative stress. *Science* **330**, 517–521 (2010).
44. Miyajima, T. et al. Loss of NQO1 generates genotoxic estrogen-DNA adducts in Fuchs Endothelial Corneal Dystrophy. *Free Radic. Biol. Med* **147**, 69–79 (2020).
45. White, T. L., Deshpande, N., Kumar, V., Gauthier, A. G. & Jurkunas, U. V. Cell cycle re-entry and arrest in G2/M phase induces senescence and fibrosis in Fuchs Endothelial Corneal Dystrophy. *Free Radic. Biol. Med* **164**, 34–43 (2021).

46. Hickson, I. et al. Identification and characterization of a novel and specific inhibitor of the ataxia-telangiectasia mutated kinase ATM. *Cancer Res* **64**, 9152–9159 (2004).
47. Phan, L. M. & Rezaeian, A. H. ATM: Main Features, Signaling Pathways, and Its Diverse Roles in DNA Damage Response, Tumor Suppression, and Cancer Development. *Genes (Basel).* **12**, 845 (2021).
48. Castedo, M., Perfettini, J. L., Roumier, T. & Kroemer, G. Cyclin-dependent kinase-1: linking apoptosis to cell cycle and mitotic catastrophe. *Cell Death Differ.* **9**, 1287–1293 (2002).
49. Kumari, R. & Jat, P. Mechanisms of Cellular Senescence: Cell Cycle Arrest and Senescence Associated Secretory Phenotype. *Front Cell Dev. Biol.* **9**, 645593 (2021).
50. Ashraf, S. et al. Dysregulation of DNA repair genes in Fuchs endothelial corneal dystrophy. *Exp. Eye Res* **231**, 109499 (2023).
51. Mah, L. J., El-Osta, A. & Karagiannis, T. C. gammaH2AX: a sensitive molecular marker of DNA damage and repair. *Leukemia* **24**, 679–686 (2010).
52. Reimann, M., Lee, S. & Schmitt, C. A. Cellular senescence: Neither irreversible nor reversible. *J. Exp. Med.* **221**, e20232136 (2024).
53. Hu, C., Zhang, X., Teng, T., Ma, Z. G. & Tang, Q. Z. Cellular Senescence in Cardiovascular Diseases: A Systematic Review. *Aging Dis.* **13**, 103–128 (2022).
54. Tomashevski, A., Webster, D. R., Grammas, P., Gorospe, M. & Kruman, I. I. Cyclin-C-dependent cell-cycle entry is required for activation of non-homologous end joining DNA repair in postmitotic neurons. *Cell Death Differ.* **17**, 1189–1198 (2010).
55. Azizi, B. et al. p53-regulated increase in oxidative-stress-induced apoptosis in Fuchs endothelial corneal dystrophy: a native tissue model. *Invest Ophthalmol. Vis. Sci.* **52**, 9291–9297 (2011).
56. Krempler, A., Deckbar, D., Jeggo, P. A. & Lobrich, M. An imperfect G2M checkpoint contributes to chromosome instability following irradiation of S and G2 phase cells. *Cell Cycle* **6**, 1682–1686 (2007).
57. Santocanale, C. & Diffley, J. F. A Mec1- and Rad53-dependent checkpoint controls late-firing origins of DNA replication. *Nature* **395**, 615–618 (1998).
58. Tercero, J. A. & Diffley, J. F. Regulation of DNA replication fork progression through damaged DNA by the Mec1/Rad53 checkpoint. *Nature* **412**, 553–557 (2001).
59. Costanzo, V. et al. Reconstitution of an ATM-dependent checkpoint that inhibits chromosomal DNA replication following DNA damage. *Mol. Cell* **6**, 649–659 (2000).
60. Heffernan, T. P. et al. An ATR- and Chk1-dependent S checkpoint inhibits replicon initiation following UVC-induced DNA damage. *Mol. Cell Biol.* **22**, 8552–8561 (2002).
61. Zhang, J. & Walter, J. C. Mechanism and regulation of incisions during DNA interstrand cross-link repair. *DNA Repair (Amst.)* **19**, 135–142 (2014).
62. Semlow, D. R., Zhang, J., Budzowska, M., Drohat, A. C. & Walter, J. C. Replication-Dependent Unhooking of DNA Interstrand Cross-Links by the NEIL3 Glycosylase. *Cell* **167**, 498–511 e14 (2016).
63. Ceccaldi, R., Sarangi, P. & D'Andrea, A. D. The Fanconi anaemia pathway: new players and new functions. *Nat. Rev. Mol. Cell Biol.* **17**, 337–349 (2016).
64. D'Amours, D. & Jackson, S. P. The Mre11 complex: at the crossroads of dna repair and checkpoint signalling. *Nat. Rev. Mol. Cell Biol.* **3**, 317–327 (2002).
65. D'Andrea, A. D. & Grompe, M. The Fanconi anaemia/BRCA pathway. *Nat. Rev. Cancer* **3**, 23–34 (2003).
66. Guleria, A. & Chandna, S. ATM kinase: Much more than a DNA damage responsive protein. *DNA Repair (Amst.)* **39**, 1–20 (2016).
67. Kumar, V. et al. Loss of NQO1 exacerbates female susceptibility to the development of Fuchs dystrophy in response to ultraviolet light. *Invest. Ophthalmol. Vis. Sci*. **61**, 1470 (2020).
68. Yamazaki, S., Miyoshi, N., Kawabata, K., Yasuda, M. & Shimoi, K. Quercetin-3-O-glucuronide inhibits noradrenaline-promoted invasion of MDA-MB-231 human breast cancer cells by blocking beta(2)-adrenergic signaling. *Arch. Biochem Biophys.* **557**, 18–27 (2014).
69. Flint, M. S., Baum, A., Chambers, W. H. & Jenkins, F. J. Induction of DNA damage, alteration of DNA repair and transcriptional activation by stress hormones. *Psychoneuroendocrinology* **32**, 470–479 (2007).
70. Najnin, R. A. et al. ATM suppresses c-Myc overexpression in the mammary epithelium in response to estrogen. *Cell Rep.* **42**, 111909 (2023).
71. Xu, B., Kim, S. T., Lim, D. S. & Kastan, M. B. Two molecularly distinct G(2)/M checkpoints are induced by ionizing irradiation. *Mol. Cell Biol.* **22**, 1049–1059 (2002).
72. Jurk, D. et al. Postmitotic neurons develop a p21-dependent senescence-like phenotype driven by a DNA damage response. *Aging Cell* **11**, 996–1004 (2012).
73. Rodier, F. et al. Persistent DNA damage signalling triggers senescence-associated inflammatory cytokine secretion. *Nat. Cell Biol.* **11**, 973–979 (2009).
74. Fumagalli, M. et al. Telomeric DNA damage is irreparable and causes persistent DNA-damage-response activation. *Nat. Cell Biol.* **14**, 355–365 (2012).
75. McConnell, B. B., Starborg, M., Brookes, S. & Peters, G. Inhibitors of cyclin-dependent kinases induce features of replicative senescence in early passage human diploid fibroblasts. *Curr. Biol.* **8**, 351–354 (1998).
76. Meek, D. W. & Anderson, C. W. Posttranslational modification of p53: cooperative integrators of function. *Cold Spring Harb. Perspect. Biol.* **1**, a000950 (2009).
77. Gire, V. & Dulic, V. Senescence from G2 arrest, revisited. *Cell Cycle* **14**, 297–304 (2015).
78. Alvarez, D. et al. IPF lung fibroblasts have a senescent phenotype. *Am. J. Physiol. Lung Cell Mol. Physiol.* **313**, L1164–L1173 (2017).
79. Yang, Y., Mufson, E. J. & Herrup, K. Neuronal cell death is preceded by cell cycle events at all stages of Alzheimer's disease. *J. Neurosci.* **23**, 2557–2563 (2003).
80. Nagy, Z., Esiri, M. M. & Smith, A. D. Expression of cell division markers in the hippocampus in Alzheimer's disease and other neurodegenerative conditions. *Acta Neuropathol.* **93**, 294–300 (1997).
81. Pelegri, C. et al. Cell cycle activation in striatal neurons from Huntington's disease patients and rats treated with 3-nitropropionic acid. *Int J. Dev. Neurosci.* **26**, 665–671 (2008).
82. Adhikari, Y., Parekh. M., Losick, V. P., Jurkunas, U. V. Polyploidy leads to senescence in an UVA-based mouse model of Fuchs Dystrophy. *ARVO Annual Meeting Abstract.* **65**, 5787 (2024).
83. Kruman, I. I. & Schwartz, E. I. DNA damage response and neuroprotection. *Front Biosci.* **13**, 2504–2515 (2008).
84. Lu, X. H. et al. Targeting ATM ameliorates mutant Huntingtin toxicity in cell and animal models of Huntington's disease. *Sci. Transl. Med* **6**, 268ra178 (2014).
85. Taylor, M. J., Thompson, A. M., Alhajlah, S., Tuxworth, R. I. & Ahmed, Z. Inhibition of Chk2 promotes neuroprotection, axon regeneration, and functional recovery after CNS injury. *Sci. Adv.* **8**, eabq2611 (2022).
86. Ruzickova, S. & Stanek, D. Mutations in spliceosomal proteins and retina degeneration. *RNA Biol.* **14**, 544–552 (2017).
87. Bhatia, V., Valdes-Sanchez, L., Rodriguez-Martinez, D. & Bhattacharya, S. S. Formation of 53BP1 foci and ATM activation under oxidative stress is facilitated by RNA:DNA hybrids and loss of ATM-53BP1 expression promotes photoreceptor cell survival in mice. *F1000Res* **7**, 1233 (2018).
88. Hirozane, T. et al. Conditional abrogation of Atm in osteoclasts extends osteoclast lifespan and results in reduced bone mass. *Sci. Rep.* **6**, 34426 (2016).

89. Herrero, A. B. & Gutierrez, N. C. Targeting Ongoing DNA Damage in Multiple Myeloma: Effects of DNA Damage Response Inhibitors on Plasma Cell Survival. *Front Oncol.* **7**, 98 (2017).
90. Weber, A. M. & Ryan, A. J. ATM and ATR as therapeutic targets in cancer. *Pharm. Ther.* **149**, 124–138 (2015).
91. Wang, Z. Regulation of Cell Cycle Progression by Growth Factor-Induced Cell Signaling. *Cells.* **10**, 3327 (2021).
92. Coppe, J. P. et al. Senescence-associated secretory phenotypes reveal cell-nonautonomous functions of oncogenic RAS and the p53 tumor suppressor. *PLoS Biol.* **6**, 2853–2868 (2008).
93. Lu, S. Y. et al. Ripe areca nut extract induces G1 phase arrests and senescence-associated phenotypes in normal human oral keratinocyte. *Carcinogenesis* **27**, 1273–1284 (2006).
94. Kuilman, T. et al. Oncogene-induced senescence relayed by an interleukin-dependent inflammatory network. *Cell* **133**, 1019–1031 (2008).
95. Lim, Y. C. et al. ATM inhibition prevents interleukin-6 from contributing to the proliferation of glioblastoma cells after ionizing radiation. *J. Neurooncol.* **138**, 509–518 (2018).
96. Benischke, A. S. et al. Activation of mitophagy leads to decline in Mfn2 and loss of mitochondrial mass in Fuchs endothelial corneal dystrophy. *Sci. Rep.* **7**, 6656 (2017).
97. Campbell, A. et al. A novel mouse model for ataxia-telangiectasia with a N-terminal mutation displays a behavioral defect and a low incidence of lymphoma but no increased oxidative burden. *Hum. Mol. Genet* **24**, 6331–6349 (2015).

Acknowledgements

The work was supported by NIH/NEI R01EY020581 (to U.V.J.). The authors thank Dr. Margot Mayer-Proschel, University of Rochester Medical Center, New York for kindly providing the Atm-WT and Atm-null mice for this study.

Author contributions

S.A., N.D., and U.V.J. designed research; S.A., N.D., Q.C. J.B., R.J.W., Y.A., A.G.G., and G.M. performed research; S.A., N.D., Q.C. J.B., and M.P., analyzed data; and S.A., N.D. and U.V.J. wrote the paper.

Competing interests

The authors declare no competing interests. Author disclosure The research presented in this manuscript is associated with an invention disclosure that has been submitted to our institution's technology transfer office. This invention disclosure relates to the application of ATM inhibitor in Fuchs Endothelial Corneal Dystrophy. For further inquiries regarding the invention disclosure or its relation to the manuscript, please contact Dr. Ula V. Jurkunas, Schepens Eye Research Institute of Massachusetts Eye and Ear, Department of Ophthalmology, Harvard Medical School, Boston, MA USA (ula_jurkunas@meei.harvard.edu).

Additional information

Supplementary information The online version contains supplementary material available at https://doi.org/10.1038/s42003-024-07179-1.

Correspondence and requests for materials should be addressed to Ula V. Jurkunas.

Peer review information *Communications Biology* thanks Brian Gabrielli, Masatoshi Takagi and the other, anonymous, reviewer for their contribution to the peer review of this work. Primary Handling Editors: Valeria Naim and Mengtan Xing.